J. Fluid Mech. (1989), *vol.* 209, *pp.* 567–589
Printed in Great Britain

Two-dimensional periodic waves in shallow water

By JOE HAMMACK,[1] NORMAN SCHEFFNER[2] AND HARVEY SEGUR[3]†

[1] Department of Aerospace Engineering, Mechanics and Engineering Sciences, University of Florida, Gainesville, FL 32611, USA

[2] US Army Engineering Waterways Experiment Station, Coastal Engineering Research Center, Vicksburg, MS 39180, USA

[3] Department of Mathematics, State University of New York, Buffalo, NY 14214, USA

(Received 31 August 1988 and in revised form 6 June 1989)

Experimental data are presented that demonstrate the existence of a family of gravitational water waves that propagate practically without change of form on the surface of shallow water of uniform depth. The surface patterns of these waves are genuinely two-dimensional and fully periodic, i.e. they are periodic in two spatial directions and in time. The amplitudes of these waves need not be small; their form persists even up to breaking. The waves are easy to generate experimentally, and they are observed to propagate in a stable manner, even when perturbed significantly. The measured waves are described with reasonable accuracy by a family of exact solutions of the Kadomtsev–Petviashvili equation (KP solutions of genus 2) over the entire parameter range of the experiments, including waves well outside the putative range of validity of the KP equation. These genus-2 solutions of the KP equation may be viewed as two-dimensional generalizations of cnoidal waves.

1. Introduction

A problem of fundamental interest in fluid mechanics is to provide an accurate description of waves on a water surface. After the experiments of Russell (1844), Airy (1845) and Stokes (1847) pioneered the theoretical study of water waves induced by gravitation using a variety of approximations to obtain practical results. In particular, they made their mathematical models tractable by assuming wave heights to be small (either linear or weakly nonlinear) and the waves to be one-dimensional. (In this paper we refer to waves as one-dimensional or two-dimensional according to whether their surface patterns are one- or two-dimensional. Their corresponding velocity fields are one dimension higher.) Even though these assumptions automatically exclude important aspects of wave motion such as breaking and two-dimensionality, much of the theoretical progress during the 140 years since the seminal work of Airy and Stokes has been linked to these two approximations. Expositions of the fundamental processes and reviews of this progress can be found in the classic books of Lamb (1932) and Stoker (1957).

Relatively little theoretical or experimental progress has been made for weakly nonlinear waves which are genuinely two-dimensional. Past research has focused primarily on short-crested waves that arise when a wavetrain is reflected at an

† Present address: Program in Applied Mathematics, University of Colorado, Boulder, CO 80309, USA.

oblique angle to its direction of propagation. The resulting wavetrain is spatially periodic in two orthogonal directions, one of which coincides with the direction of pattern propagation. (Such a wave pattern is also symmetric about the direction of propagation, and it can be approximated by the superposition of two identical wavetrains propagating at oblique angles to one another.) In deep water Hsu, Tsuchiya & Silvester (1979) and Hsu, Silvester & Tsuchiya (1980) presented two-dimensional generalizations of Stokes' expansion for short-crested waves, following earlier work by Fuchs (1952) and Chappelear (1959, 1961). Roberts (1983) and Roberts & Peregrine (1983) also examined properties of short- and long-crested (weakly two-dimensional) waves. Numerical calculations of Fourier coefficients to represent short-crested waves in deep water have been presented by Roberts & Schwartz (1983) and Bryant (1985). In order to explain the experimental observations of Su *et al.* (1982) and Su (1982), McLean (1982*a*) analysed the stability of one-dimensional waves in deep water to two-dimensional disturbances and Meiron, Saffman & Yuen (1982) extended earlier work (Saffman & Yuen 1980) on bifurcations of Stokes' waves.

In shallow water, the oblique interactions of one-dimensional cnoidal and solitary waves were studied analytically by Benney & Luke (1964) and Miles (1977*a*, *b*), and experimentally by Melville (1980). Benney & Roskes (1969) and McLean (1982*b*) showed that one-dimensional sinusoidal wavetrains are unstable to two-dimensional perturbations. Su *et al.* (1981) presented experimental data which showed the enhancement of instabilities with decreasing water depths. Bryant (1982) calculated Fourier coefficients numerically to examine short-crested waves; Le Mehaute (1986) examined their maximum wave heights. Bridges (1987*a*, *b*) used bifurcation theory to find two-dimensional cnoidal standing-waves. Segur & Finkel (1985) presented a two-dimensional generalization of cnoidal waves in shallow water based on a multi-parameter family of exact solutions of the equation of Kadomtsev & Petviashvili (1970, hereinafter referred to as KP). These solutions are also spatially periodic in two directions; however, the directions need not be orthogonal, so that both symmetric and asymmetric patterns are possible. Segur & Finkel conjectured that members of this family of periodic, nonlinear, two-dimensional waves represent 'typical' periodic waves in shallow water. Their work motivated this experimental study.

The two major results of the present study are as follows. Experiments demonstrate the existence of a family of genuinely two-dimensional, shallow-water waves that are fully periodic in two spatial directions and time; their surface patterns are hexagonal. These waves are easy to generate and are extremely robust, maintaining their form up to breaking amplitudes. They propagate with practically no change in form for distances up to 25 wavelengths (the basin length), even though depth variations in the basin are as large as the wave amplitudes. Secondly, the KP model of these waves is remarkably accurate. This accuracy persists even for experimental waves well outside the putative range of validity of the KP equation.

An outline of the paper is as follows. The KP equation is discussed briefly in §2 along with its two-dimensional periodic solutions. An algorithm is presented for choosing parameter values of these solutions so that they 'best' represent the measured waves. An error measure is then introduced to quantify how accurately the KP solutions describe the measured waves. Experimental facilities and procedures for generating two-dimensional waves are described in §3. Detailed experimental results are presented in §4, along with comparisons of these results with KP theory

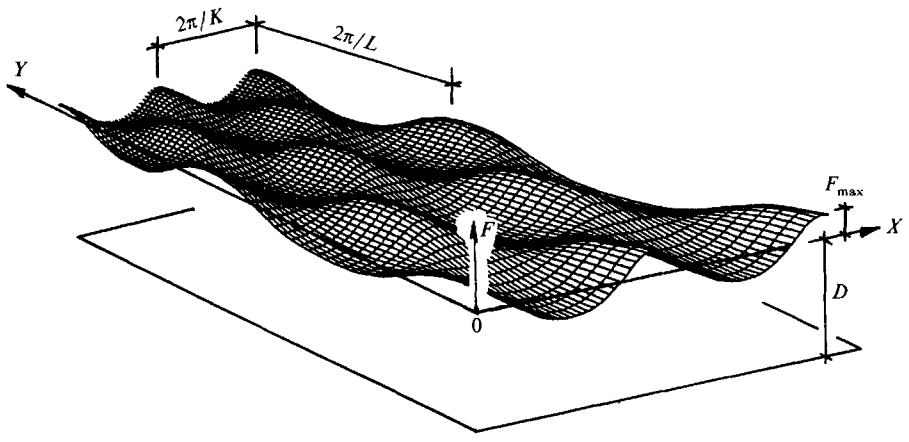

FIGURE 1. Definition sketch of the fluid domain.

and another theoretical model based on the linear superposition of cnoidal waves. Conclusions are summarized in §5.

2. Summary of KP theory

The equation of Kadomtsev & Petviashvili (1970) is a nonlinear differential equation of the form

$$(f_t+6ff_x+f_{xxx})_x+3f_{yy}=0. \tag{1}$$

Thorough discussions of the KP equation and its relation to waves in shallow water have been presented elsewhere (e.g. Segur & Finkel 1985), so we merely summarize the main results here. The KP equation describes the slow evolution of gravity-induced waves on water of uniform depth when the waves are assumed to be (i) long, (ii) weakly two-dimensional (with the x-direction dominant), and (iii) moderate in amplitude; all three effects are supposed comparable in magnitude. In terms of the dimensional quantities shown in figure 1, these three assumptions formally require

$$(KD)^2 \ll 1, \quad (L/K)^2 \ll 1, \quad (F_{\max}/D) \ll 1, \tag{2}$$

where (K, L) are typical wavenumbers in the (X, Y) directions, $F_{\max}$ is a vertical scale of the surface deformation from its reference position and D is the reference water depth, defined so that periodic waves have zero mean-amplitude. The scaled variables in (1) are related to dimensional quantities according to

$$x=\sqrt{\epsilon}(X-(gD)^{\frac{1}{2}}T)/D, \quad y=\epsilon Y/D, \tag{3a, b}$$

$$t=(\epsilon^3 gD)^{\frac{1}{2}}T/(6D), \quad f=3\epsilon F/(2D)+O(\epsilon^2), \tag{3c, d}$$

where g is the gravitational force per unit mass. (Surface tension could also be included in this description but is omitted here.) The three assumptions of (2) that underlie the KP equation are inherent in the limit $\epsilon \to 0$. Herein, we set $\epsilon = 1$ in order to compare with definite experiments, with the effect that a free parameter of the solution (termed k later) is required to be small for formal validity of the model.

The KP equation is a natural generalization of the famous equation of Korteweg & de Vries (1895)

$$f_t+6ff_x+f_{xxx}=0, \tag{4}$$

from one spatial dimension to two. It inherits many of the remarkable properties of the KdV equation, including the existence of an infinite hierarchy of periodic and quasi-periodic solutions with the form

$$f(x,y,t) = 2\partial_x^2 \ln \Theta_N, \tag{5}$$

where Θ_N is a Riemann theta function of genus N. These solutions were discovered by Krichever (1977), and were made computational for low genera by Dubrovin (1981) and Segur & Finkel (1985). For the genus-2 solutions of interest herein, Θ_2 is given by a double Fourier series,

$$\Theta_2(\phi_1,\phi_2;\boldsymbol{B}) = \sum_{m_1=-\infty}^{\infty}\sum_{m_2=-\infty}^{\infty} \exp\left[\tfrac{1}{2}(m_1^2 b + 2m_1 m_2 b\lambda + m_2^2(b\lambda^2+d)) + \mathrm{i}(m_1\phi_1 + m_2\phi_2)\right], \tag{6}$$

where the phases ϕ_1 and ϕ_2 are given by

$$\phi_j = k_j x + l_j y + \omega_j t + \phi_{j0} \quad (j=1,2). \tag{7}$$

ϕ_{10} and ϕ_{20} are phase constants, and the real-valued parameters (b,λ,d) define the elements of a Riemann matrix $\boldsymbol{B}$ according to

$$\boldsymbol{B} = \begin{bmatrix} b & b\lambda \\ b\lambda & b\lambda^2+d \end{bmatrix}, \tag{8}$$

provided b and d are negative. These solutions contain eleven parameters including two (ϕ_{10},ϕ_{20}) that represent translational symmetry and nine $(b,\lambda,d,k_1,k_2,l_1,l_2,\omega_1,\omega_2)$ that we refer to as dynamical. Of the nine dynamical parameters, six are free since the KP equation provides three algebraic constraints among the nine.

Segur & Finkel (1985) presented an algorithm to choose the six dynamical parameters so as to obtain real-valued, bounded KP solutions of genus 2 that are genuinely two-dimensional. In these first experiments we limit our attention to a three-parameter subset of genus-2 solutions that are invariant under the transformation $y \to -y$; we call waves in this subset symmetric. In order to obtain a symmetric solution, first choose the parameters (b,λ,d) so that

$$-\infty < b < 0, \quad 0 < \lambda < 1, \quad d = b(1-\lambda^2). \tag{9a,b,c}$$

Condition (9*b*) differs from the normalization of λ given by Segur & Finkel (1985): either is legitimate, and (9*b*) is convenient for comparison with our experiments. Symmetry is imposed by taking (9*c*) and by requiring

$$k_1 = k_2 (=:k), \quad l_1 = -l_2 (=:l). \tag{10a,b}$$

The last parameter to choose is k, which fixes the scaling symmetry in (1) and the x-wavelength of the entire pattern; without loss of generality, $k > 0$. Then one shows from the algebraic constraints that

$$\omega_1 \equiv \omega_2 (=:\omega), \tag{10c}$$

so that the solution is truly symmetric. The remaining two algebraic constraints define $(l/k^2)^2$ and (ω/k^3). Numerical results indicate that these quantities are always real for symmetric solutions, and that $l \neq 0$ so the solution is genuinely two-dimensional. Finally, choosing (ϕ_{10},ϕ_{20}) fixes the origin of the coordinate system and completes the specification of the solution.

Every KP solution of genus 2 obtained in the manner outlined above is bounded,

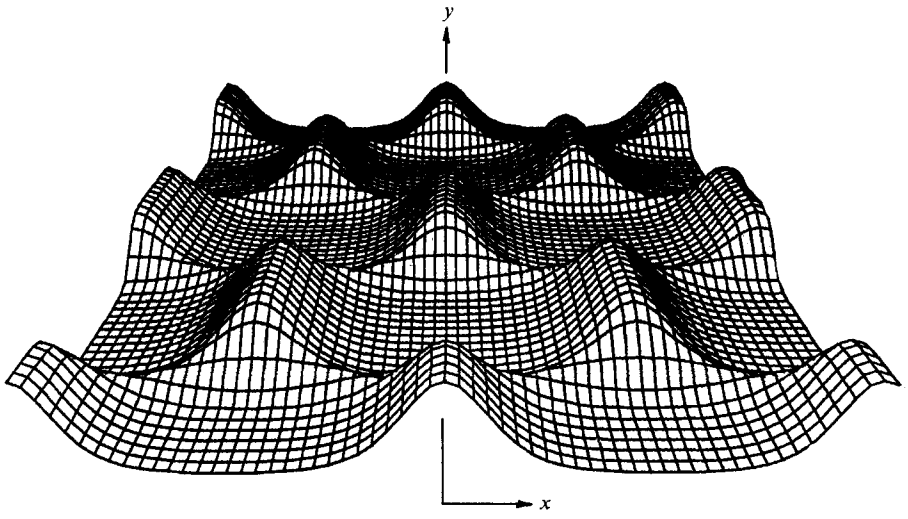

FIGURE 2. Symmetric KP solution of genus 2: $b = -6.20$, $\lambda = 0.55$, $\mu = 0.90$ (corresponds to experiment KP1007).

real-valued, symmetric, and genuinely two-dimensional. The x- and y-axes are directions of periodicity, and the entire spatial pattern is obtained by a periodic tiling of rectangles with dimensions $(2\pi/k \times 2\pi/l)$. The pattern is stationary in a coordinate system moving in the x-direction with speed (ω/k), corresponding to a dimensional speed of $(gD)^{\frac{1}{2}}(1+\omega/6k)$ in laboratory coordinates. The KP model of water waves attains formal asymptotic validity in the limit $k \to 0$, with $(l/k^2)^2$ and (ω/k^3) finite. However, we will demonstrate reasonable agreement between theory and experiment even when k is not very small.

Figure 2 shows a symmetric genus-2 solution for one choice of parameters; two spatial periods in each direction are shown. The dominant feature of the wavefield is the array of large-amplitude crests that are normal to the x-axis. These large crests are connected by saddle-like regions of smaller amplitudes to form a hexagonal surface pattern. It is evident that the wavefield is two-dimensional, but also that it contains large regions in which the waves are effectively one-dimensional. In these one-dimensional regions the waves can be approximated by a KdV cnoidal wavetrain, but obviously no such one-dimensional approximation could be uniformly valid in space. An appealing feature of genus-2 solutions of the KP equation is that one-dimensional regions fit naturally into obviously two-dimensional wave patterns.

Figure 3 shows another symmetric KP solution of genus 2 for a different choice of free parameters. This particular solution lacks the large one-dimensional regions evident in figure 2, but the persistent hexagonal pattern shows the qualitative similarity of the two solutions. The dominant wave crests are still those normal to the x-axis; crests in the saddle regions are barely discernible. In fact, every symmetric KP solution of genus 2 is qualitatively similar to those in figures 2 and 3. Different solutions correspond simply to different lengthscales in the x, y and f (vertical) directions. One specifies these lengthscales by the choice of k, λ and b, more or less respectively. This correspondence forms the basis for choosing genus-2 solutions to represent measured wave data, as we discuss next.

In order to test KP solutions of genus 2 as a model of experimental water waves,

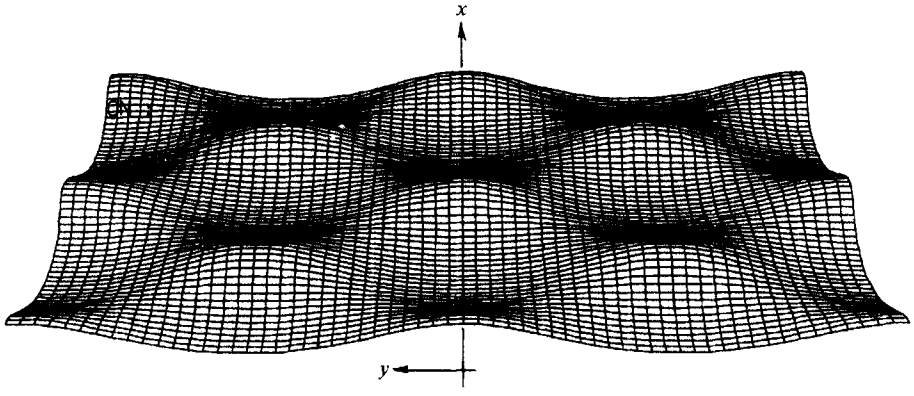

FIGURE 3. Symmetric KP solution of genus 2: $b = -5.55$, $\lambda = 0.25$, $\mu = 0.80$ (corresponds to experiment KP3007).

it is necessary to choose the five free parameters $(b, \lambda, k, \phi_{10}, \phi_{20})$ of a solution that best represents the measured wavefield. In the experiments described below, approximate measurements of the x- and y-wavelengths and more accurate measurement of the t-period and the maximum wave amplitude were available. These data led to the following optimization scheme for fitting genus-2 solutions. First, estimates of k and l are obtained from the measured x- and y-wavelengths. For any λ, b can be chosen in order to make the maximum amplitude of the computed and measured waves agree. The value of k is then varied in order to match the computed and measured wave periods. Finally, λ is varied until the computed and measured y-wavelengths agree. The scheme is repeated if the variation of one parameter creates too large a discrepancy in an earlier match; the allowable range for each parameter depends on the accuracy of experimental measurement. (Based on the experiments described in §3, we require agreement to within 5% for $f_{\max}$, 3% for t-periods, and 10% for y-wavelengths, when that length is completely resolved by the overhead photographs.) Once (b, λ, k) are chosen in this manner, the phases (ϕ_{10}, ϕ_{20}) are chosen to optimize the agreement between computed and measured wave patterns.

The above surface-fitting algorithm converged rapidly, both for inferring (b, λ, k) from a calculated KP solution and for fitting experimental waves, which have no 'correct' values of b, λ and k. It is important to recognize that only three measurements are needed to determine (b, λ, k), from which the entire wavefield can be reconstructed, up to translation. Once these parameters are chosen using three measurements, any other measurement of the wavefield is predicted by the theory.

In order to quantify the accuracy of the chosen KP solutions in describing the measured waves, it is useful to choose some definite measure of goodness-of-fit. Moreover, an error measure will allow us to rank order the experiments and provide insight into the experimental parameter ranges for which KP theory is valid. A traditional measure of error is the r.m.s. (root-mean-square) of the differences between data and theory. Given a symmetric, periodic surface wave with zero mean in shallow water, let $\zeta_{i,j}$ represent measured values of the wave amplitude in an array of points (x_i, y_j) in the spatially periodic rectangle. Let $f_{i,j}$ denote the values given by the corresponding symmetric, periodic KP solution of genus 2 at the same points. (It

follows from (5) that the solution has zero mean as well.) Then a normalized r.m.s. error σ between $f_{i,j}$ and $\zeta_{i,j}$ may be defined as

$$\sigma = \frac{(\sum_{i,j} (\zeta_{i,j} - f_{i,j})^2)^{\frac{1}{2}}}{(\sum_{k,l} (\zeta_{k,l})^2)^{\frac{1}{2}}}. \tag{11}$$

According to (11), a value $\sigma = 0$ corresponds to no error while $\sigma = 1$ is equivalent to using no theory at all, i.e. $f_{i,j} = 0$. (Of course, a non-zero theory could also give $\sigma = 1$.) Note that σ is an unbounded error measure; hence, it is misleading to think of σ in terms of percentage error. It is worth emphasizing that the surface-fitting algorithm described above does not involve the error measure so that no explicit attempt is made to minimize σ (see Appendix A).

3. Experimental facilities and procedures

Experiments were conducted at the Coastal Engineering Research Center (CERC), US Army Engineer Waterways Experiment Station, in Vicksburg, Mississippi. The facilities used for these experiments include (i) a wave basin, (ii) a directional wave generator, (iii) wave gauges, (iv) a camera system, and (v) a computer system for control of the wavemaker and data acquisition. Both the basin and wave generator were new, and the time available for their use was limited. The newness of the equipment masked some limitations that did not become apparent until experiments were well underway. Also, the newness (at least to the authors) of measuring two-dimensional wave patterns did not allow us to preplan the experiments in an optimal way. Even so, the reported data have the refinement and resolution necessary to test both the existence of two-dimensional, steady, spatially periodic waves and the accuracy of KP theory in predicting their form. The experiments also provide qualitative information on the stability of the waves. Both the equipment and procedures are described in more detail by Scheffner (1988).

3.1. *Overview of facilities*

Figure 4 shows a schematic drawing of the laboratory facilities. The enclosed wave basin was 30 m wide and 56 m long with a poured-slab concrete floor and concrete block sidewalls. A water depth of $D = 30$ cm was used in all experiments. The concrete floor of the basin was not flat; bathymetry measurements yielded depth variations up to ± 3 cm. A rectangular grid of points was marked on the basin floor to serve as benchmarks for placement of wave gauges and for reduction of photographic data. A 4 m width of rubberized horsehair was placed along the 30 m endwall opposite the wavemaker in order to absorb wave energy. No absorption material was used along the basin's 56 m sidewalls.

The directional wave generator was located along one of the 30 m endwalls of the basin. This segmented wavemaker consisted of 60 vertical piston-type paddles, each with a width $W = 45$ cm, which penetrated the entire water column. (The wavemaker spanned the central 27 m of the 30 m endwall.) The paddles were not sealed against leakage at the basin floor; however, flexible membranes between adjacent paddles inhibited flow there and acted to smooth the face of the wavemaker. Horizontal actuators were located at the joints between paddles so that the wavemaker motion was determined by 61 push–pull points. The motion for each of the 61 actuators was

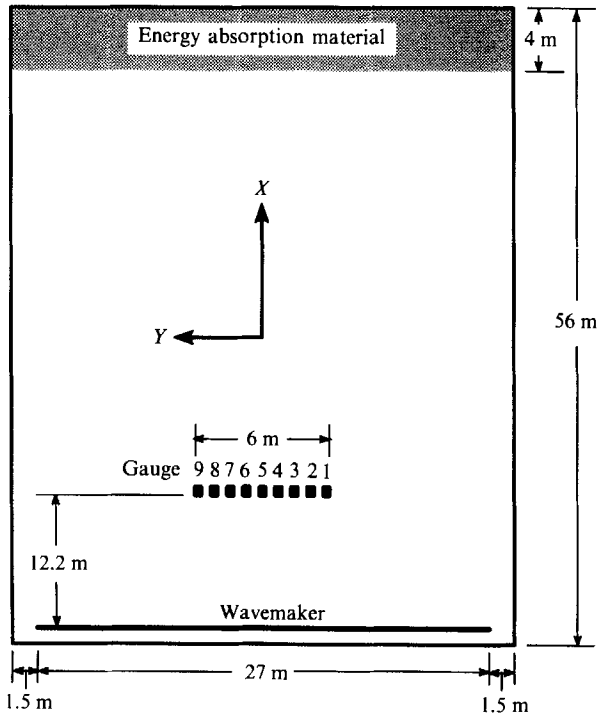

FIGURE 4. Schematic drawing of the wave basin.

programmable and servo-controlled with position feedback. The maximum displacement of an actuator was 30 cm. Command signals corresponding to the desired time-displacement histories for each of the actuators were provided by a dedicated DEC VAX-750 computer system that was also used to collect and analyse data.

Two types of measurements were made during the experiments. First, parallel wire, resistance-type gauges measured the vertical deformation $F(X, Y, T)$ of the water surface from its quiescent position at nine fixed locations, which were spaced 75 cm apart and were aligned in a linear array parallel to and 12.2 m from the wavemaker, as shown in figure 4. The gauge array was placed astride the basin's centreline (X-axis). The 6 m length of the gauge array was sufficient in all experiments to span at least half a Y-wavelength for the generated wave patterns. The analog signals from these gauges were digitized (without prior filtering) at a rate of 50 Hz by the computer system. All of the gauges were statically calibrated prior to each experiment under control of the computer system. Gauge calibrations were linear over the full 15 cm of wave height they could measure.

Secondly, photographs of the surface wave patterns in the vicinity of the gauges were made using two Hasselblad 500 EL/M 70 mm cameras. These cameras were placed 6 m apart, astride the basin centreline, and 7 m above the gauge array; their focal planes were parallel to the quiescent water surface. (The wave gauges were removed during photography.) The building was first darkened and then illuminated for photography by two 8000 W-s strobe lights located just above the wavemaker and pointing horizontally in the X-direction. Hence, the photographs show wave crests as regions of strong gradients in grey level with the front face of a wave darkest (e.g. see figure 7). The fields of view of the two cameras overlapped so that a mosaic of simultaneous photographs provide a picture of the wave pattern in an area with

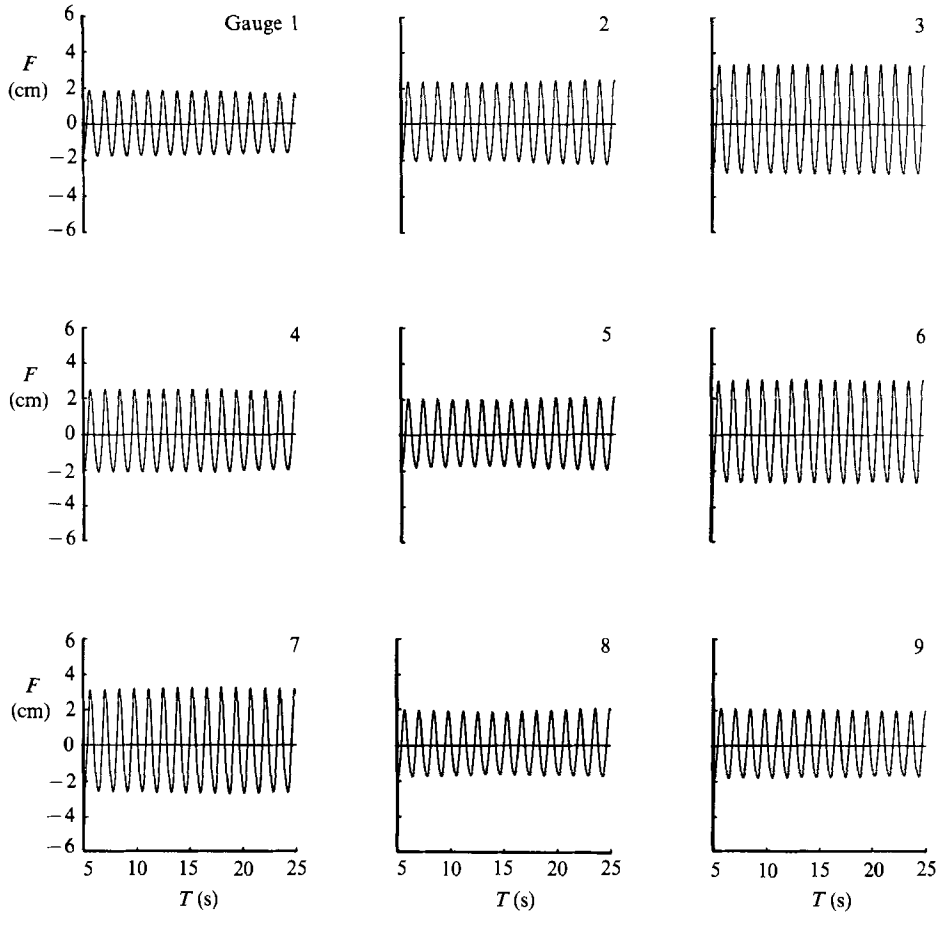

FIGURE 5. Wave profiles at each of the nine gauges for the underlying cnoidal (genus-1) wavetrain used in the experiments of series KPxx07.

a size of approximately 7.0×12.2 m. This area was sufficient in all but three experiments (KP10xx) to capture one spatial wavelength in the Y-direction. The known geometry of the camera system and the photographic printing procedures enabled horizontal distances in the wave pattern to be measured from photographs with an accuracy of about 10%. In addition to these semi-quantitative photographs, a video tape of one series of experiments was made, showing the evolution of the entire wave pattern. (This video tape is available by contacting N. Scheffner at the address given above.)

3.2. *Generation of genus-1 waves*

The clean generation of freely propagating waves in the laboratory requires the wavemaker to impart a velocity field to the water column which is similar to that occurring naturally. Since the vertical distribution of velocity is relatively uniform for long waves, piston-type wavemakers, which penetrate the water depth and move horizontally, are generally used. Excellent results for generating genus-1 (cnoidal) waves have been presented by Goring & Raichlen (1980) who used a single piston in a narrow channel. In their procedure, the programmed motion of the piston fully accounted for the finite displacement of the wavemaker. In order to calibrate the

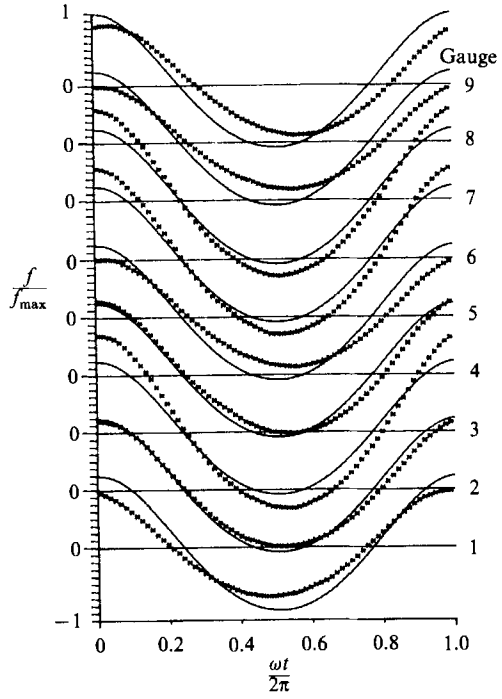

FIGURE 6. One-dimensional slices through the surface pattern of the underlying cnoidal wavetrain used in the experiments of series KPxx07: ——, theoretical, based on average measured wave properties; ***, experimental.

laboratory facility, the procedure of Goring & Raichlen was implemented using the segmented wavemaker. (It also turned out that these genus-1 waves were essential in the clean generation of genus-2 waves, as will be discussed in §3.3.) Figure 5 shows the time series $F(X_0, Y_n, T)$, with $X_0 = 12.2$ m and $n = 1, \ldots, 9$ corresponding to each of the wave gauges, when a (one-dimensional) cnoidal wavetrain was generated and directed along the X-axis. The stroke amplitude of the paddle was $S = 5$ cm and the wavemaker period was $\tau = 1.38$ s. (The wavelength, Λ, in the direction of propagation and the elliptic modulus, M, are listed in table 1 under experiments KPxx07.) Ideally, wave amplitude and phase should be identical at each gauge site in figure 5 and the amplitudes should be steady. Weak unsteadiness is apparent at each gauge site. Discrepancies in amplitudes among gauge sites are also obvious; variations up to 26% in negative amplitudes and 33% in positive amplitudes are evident. Variations in wave phases between gauge sites also exist. We attribute both discrepancies primarily to the spatial non-uniformities in water depth between the wavemaker and the gauge array. However, it should be emphasized that the stability of cnoidal waves to two-dimensional perturbations has not been established theoretically, or experimentally in wide basins. Hence, some of the variations among gauge sites in figure 5 may be a consequence of instabilities. (As noted in §1, sinusoidal waves in shallow water are unstable to two-dimensional perturbation.)

In order to quantify the differences among wave gauge records in figure 5, the measured results during a single wave period are compared with those of a theoretical genus-1 wave in figure 6. The theoretical wave is based on the average values of the crest-to-trough height (H), period, and starting phase of the measured waves. The wave beginning near $T = 15$ s was chosen from each of the nine gauge records of

Experiment	Wavemaker period† τ (s)	Paddle phase shift‡ α (°)	Directed wave angle β (°)	Directed wavelength‡ Λ (f)	Elliptic modulus M
KP1007	1.38	10	7.4	7	0.66
KP1507	1.38	15	11.0	7	0.66
KP2007	1.38	20	14.5	7	0.66
KP3007	1.38	30	21.3	7	0.66
KP4007	1.38	40	27.4	7	0.66
KP1011	1.95	10	11.5	11	0.90
KP1511	1.95	15	17.0	11	0.90
KP2011	1.95	20	22.2	11	0.90
KP3011	1.95	30	31.4	11	0.90
KP1015	2.55	10	15.5	15	0.97
KP1515	2.55	15	22.6	15	0.97
KP2015	2.55	20	29.1	15	0.97

TABLE 1. Generation parameters for the underlying cnoidal waves in each experiment: $S = 5$ cm, $D = 30$ cm

† The measured wave periods of cnoidal wavetrains are equal to those of the command signals.

‡ Note that the identification label for each experiment gives the angle α in the first two digits followed by the wavelength in feet in the last two digits.

figure 5 for analysis; similar results are obtained for other waves in the record. Based on the r.m.s. error defined in (11), we find $\sigma = 0.24$ between the measured and theoretical waves of figure 6. One can interpret this value as typical of the experimental error inherent in our laboratory facility.

3.3. *Generation of genus-2 waves*

It was found experimentally that genus-2 waves could be generated best by letting them evolve from two, obliquely interacting, genus-1 wavetrains input at the wavemaker. Direct generation was also tried; each of the 61 actuators was programmed using KP theory suitably modified to account for the finite displacement of each actuator. This method produced very unsatisfactory results. The wavefields were unsteady and differed in their qualitative features from expected genus-2 behaviour. The difficulty with direct generation appeared to result from the narrowness of the saddle regions and the steep wave angles there required by KP theory. The paddle widths ($W = 45.75$ cm) were simply too large to resolve waves in the saddle regions.

The final procedure adopted for generation of genus-2 waves was as follows. First, the wavemaker was programmed to generate a single cnoidal wavetrain using the procedure of Goring & Raichlen (1980); the stroke amplitude S and period τ of the paddle were prescribed and the wave was directed along the X-axis. This wavetrain was measured, and then the periodic command signals to adjacent actuators were phase lagged by an angle α in order to generate the same wavetrain directed at an angle $(+\beta)$ to the X-axis. (The relation between α and β is given by $\beta = \arctan(\alpha\Lambda/360W)$, in which all angles are in degrees. The angle β of the cnoidal wavetrains is related to the parameters of the genus-2 solutions by $\beta = \arctan(l/k)$.) Command signals for the same wavetrain at an angle $(-\beta)$ to the X-axis were then constructed, and the two signals were superposed to produce a final command signal. It is noted that this method of wave generation also provides a direct test of a genus-2 waves as a model for the oblique interaction of two identical cnoidal wavetrains in shallow water.

Twelve experiments were performed for three different wavemaker periods τ and a wide range of angles β; the paddle stroke for each of the underlying cnoidal wavetrains was $S = 5$ cm in all experiments. Generation parameters S, τ and α are summarized in table 1, which also shows the directed angle β, the directed wavelength Λ, and the elliptic modulus M for the underlying cnoidal waves of each experiment. The chosen stroke was the maximum allowable in order to avoid wave breaking in any of the twelve experiments. (The experiments with the shortest underlying genus-1 waves, i.e. KPxx07, were nearest breaking.) Large wave heights were used in order to make the photographic data more definitive. Consequently, these waves were not necessarily small, contrary to one of the theoretical assumptions discussed in §2. Only a portion of the data from the twelve experiments is presented here. A complete set of data can be found in Scheffner (1988).

Since the two-dimensional experimental waves evolved from obliquely interacting genus-1 waves, we cannot expect better results with the genus-2 solutions than obtained for the single cnoidal wavetrain of figures 5 and 6. Although the depth variations in the wave basin were a major perturbation to the generated wave fields, there were other perturbations as well. Clearly the method used to generate genus-2 waves introduced extraneous waves since the velocity distribution along the wavemaker was not that required by KP theory. It has already been noted that the basin sidewalls were 1.5 m from the ends of the wavemaker. Hence, diffraction effects occurred at the ends of the finite-width wavetrains, even when they were directed along the basin axis. These effects were exaggerated further when wavetrains were directed at angles to the X-axis. Diffraction followed by reflection (and reflection followed by diffraction) at the sidewalls contaminated the wavefield and led to further unsteadiness in the measurements. All of these latter effects increase for large angles β so that one expects a corresponding decrease in the accuracy of any steady-state theory for experiments with large angles.

4. Presentation and discussion of results

Experimental data are first presented to demonstrate the existence and nature of the symmetric periodic wave patterns that evolve from two obliquely interacting cnoidal wavetrains. Once the qualitative similarities between the experimental waves and exact KP solutions of genus 2 shown in §2 are established, a quantitative comparison of KP theory and wave gauge data is presented.

4.1. *Two-dimensional periodic experimental waves*

In order to demonstrate the existence of fully periodic waves, mosaics of two overhead photographs for each of three experiments are presented in figure 7. Recall from §3 that the strobe lighting for each photograph was located at the wavemaker and pointed in the positive X-direction. Hence, front faces of wave crests appear dark while the rear faces appear light.

The similarities of the hexagonal wave patterns in figure 7 with those of the theoretical genus-2 waves in figures 2 and 3 are obvious. (In fact, the computed waves of figures 2 and 3 represent the best-fit solutions for the experimental waves in figure 7 (a, c), respectively.) The wave pattern in experiment KP1007 of figure 7 (a) is dominated by nearly one-dimensional wave crests that propagate in the direction of the pattern (along the X-axis). Similar wave crests are also the most pronounced feature of the wave patterns in experiments KP2007 and KP3007 of figure 7 (b, c),

respectively. However, the lengths of these crests decrease dramatically as the angle of the underlying genus-1 waves increases from $\beta = 7.4°$ in figure 7(*a*) to $\beta = 21.3°$ in figure 7(*c*). Based on the method of generating the wave patterns in figure 7, the dominant wave crests may be interpreted as resulting from the nonlinear interaction between crests of the underlying genus-1 waves. This is the periodic analogy of the Mach stem found by Miles (1977*a*) for obliquely interacting solitary waves. Henceforth, we refer to these dominant crests as interaction regions. As in the genus-2 solutions of figures 2 and 3, the interaction regions in figure 7 are connected spatially by saddle regions to form hexagonal surface patterns. These saddle regions may be interpreted qualitatively as remnants of the two cnoidal waves input by the wavemaker. Even though the input cnoidal waves make angles with the X-axis ranging from 7.4° to 21.3° in figure 7, crests in the saddle regions remain at an angle of approximately 45° in each experiment. Since the X-wavelength of the hexagonal pattern increases only slightly as the input angle β increases, the width in the Y-direction of the saddles remains small, about 1.5 m in figure 7. (As noted in §3.2, this behaviour was the main reason that direct generation of genus-2 waves by the segmented wavemaker was unsatisfactory.) Clearly, the wave patterns of figure 7 are genuinely two-dimensional and qualitatively similar to the genus-2 waves described in §2.

Two other aspects of the wavefields in figure 7 should be noted. First, the sharp contrast in grey level (light to dark) occurring across portions of the wave crests in the interaction region indicates that the crests are very peaked there. In fact, there was other experimental evidence that all of these crests in experiments KPxx07 were very near their breaking height. For example, a 10% increase in stroke amplitude caused the waves of KP1007 to break. Second, wave crests in the interaction regions of figure 7 exhibit some spatial snaking along their crests: this is especially obvious in experiment KP1007 of figure 7(*a*). This behaviour probably results from the varying water depth between the wavemaker and photograph site, which gives rise to different arrival times for a phase position along a crest. (Recall that this effect was observed for the genus-1 waves shown in figure 6.) The snaking of wave crests in figure 7 was manifest temporally as a to-and-fro wobbling of crests during propagation. (The latter effect is clearly visible in the video of the experiments.)

Figure 8 shows a portion of the wave gauge data obtained during experiment KP3007. Wave profiles are presented for each of the nine gauges whose spatial locations are shown in figure 7(*c*). Note that the 6 m array of gauges spans slightly more than one Y-wavelength. Gauges 1 and 2 are located in interaction regions with gauge 2 nearer the saddle. Crest-to-trough wave heights H decrease slightly between gauges 1 and 2, and then decrease dramatically at gauge 3, which is located near the centre of a saddle region. According to KP theory, gauges in saddle regions should measure two identical crests per wave period. Gauge 3 shows that two crests are present in each wave period; however, their amplitudes are not identical. As we continue traversing the gauge array, moving from interaction region to saddle and back, increases and decreases in wave heights occur. All of the wave gauges exhibit some unsteadiness in amplitude. In the saddle data of gauges 3 and 7, this unsteadiness is also manifest by the gradual emergence of the second crest expected there. Finally, we note that the ratio of maximum wave height to water depth occurs at gauge 8, and has a value $H/D \approx 0.42$. This value is considerably less than the accepted breaking criterion for one-dimensional waves (e.g. $H/D \approx 0.8$, see Sarpkaya & Isaacson 1981); however, as already noted, other experiments indicate that all of the waves of figure 7(*c*) are very near their limiting heights.

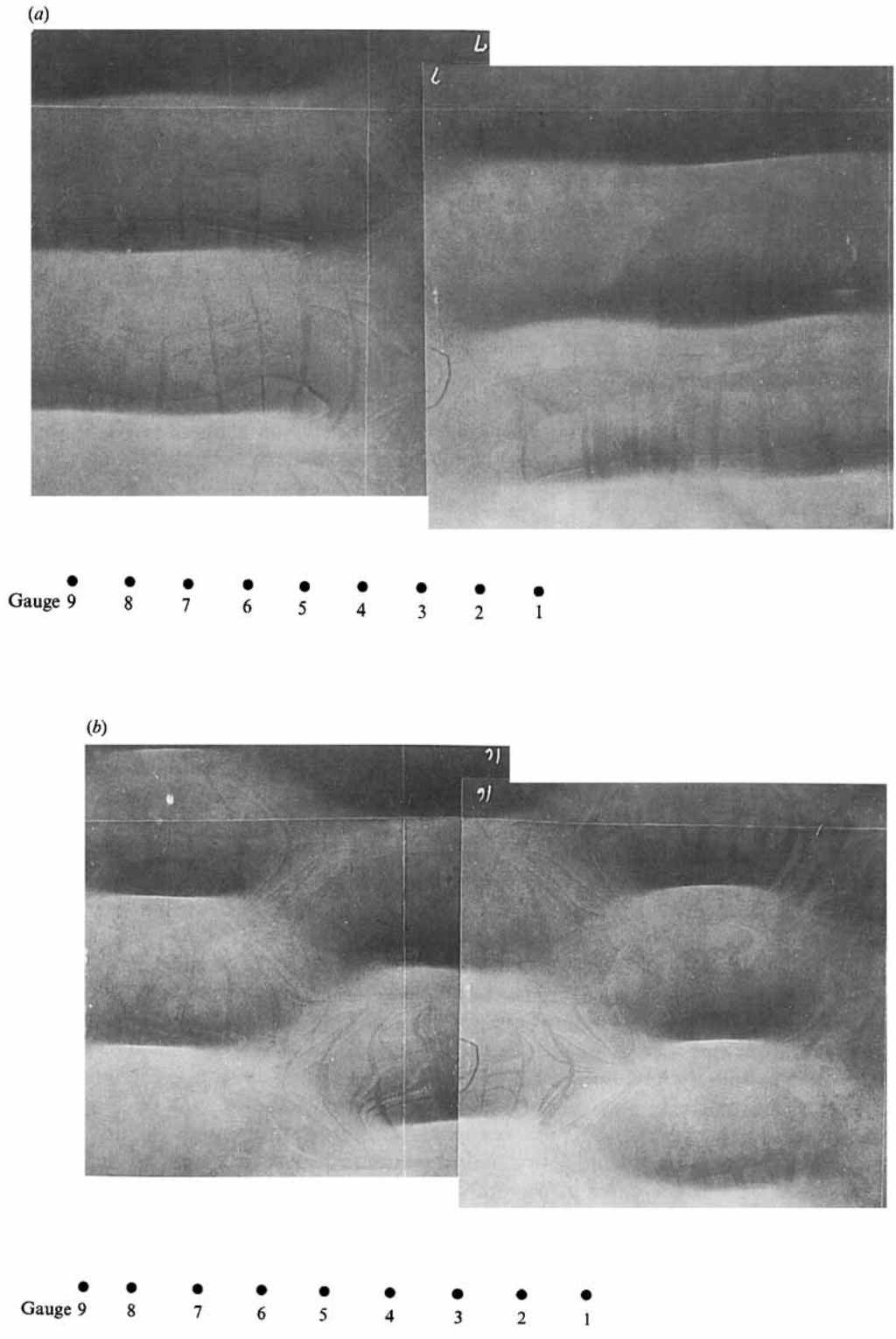

FIGURE 7. (*a*) and (*b*). For description see opposite.

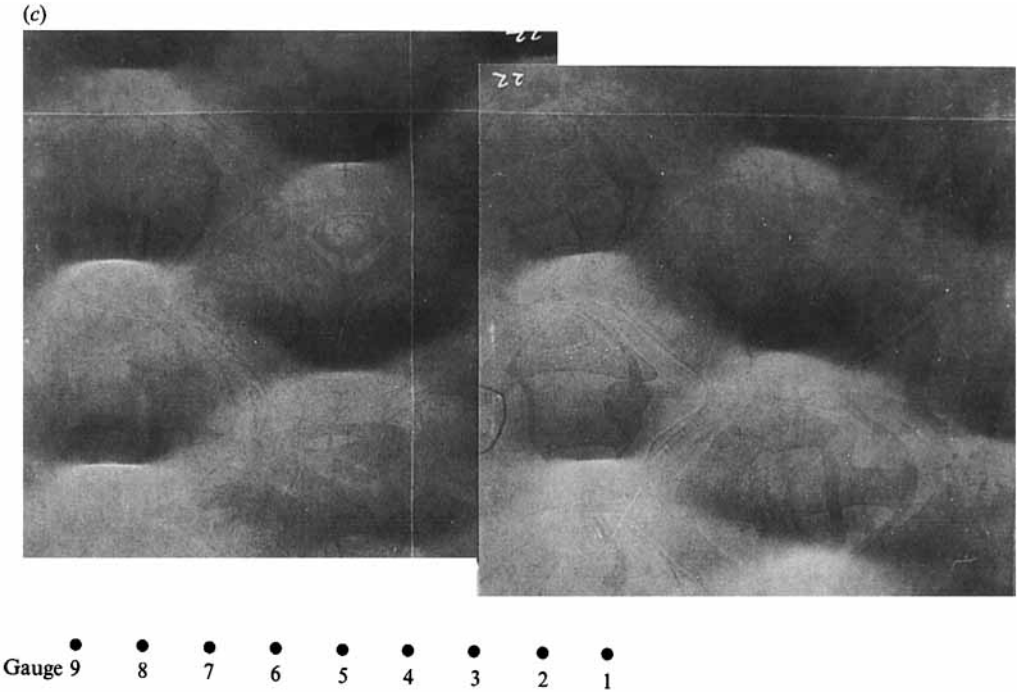

FIGURE 7. Mosaics of two overhead photographs showing water surface patterns. Wave gauge positions are also indicated. (*a*) Experiment KP1007; (*b*) experiment KP2007; (*c*) experiment KP3007.

4.2. *Comparison of experimental waves with KP theory*

In order to test the applicability of KP solutions of genus 2 to model fully periodic water waves, it is necessary to choose the three dynamical parameters (b, λ, k) and two nondynamical parameters (ϕ_{10}, ϕ_{20}) which yield a best-fit KP solution for a particular experiment. (Recall that b, λ and k correspond to lengthscales of the solution in the vertical, Y-, and X-directions, more or less respectively.) Such a surface-fitting algorithm based on the photographic and wave gauge data available in this study was outlined in §2. Results of the algorithm are presented for all twelve experiments in table 2 which shows the KP parameters of the best-fit solutions and the corresponding error σ between the KP model and the measured waves. It should also be noted that the photographs in experiments KP10xx did not capture a full Y-wavelength; hence, these data were supplemented by direct observation of the waves.

Quantitative comparisons between measured and theoretical wave profiles at each of the nine gauge sites are presented in figure 9 for three of the twelve experiments. These experiments are representative of the twelve conducted in the sense that one from each series of experiments is shown and that they span a wide range in error measure (see table 2) from $\sigma = 0.27$ in KP1515 to $\sigma = 0.51$ in KP1011. The wave profiles $f/f_{\max}$ are shown for simultaneous measurements during one wave period; this wave period is typical of the entire wave record. (Results for this wave period were compared to those for other periods in the record and to those for an average period constructed from a five-wave interval of the record. Details of these comparisons are presented by Scheffner 1988.)

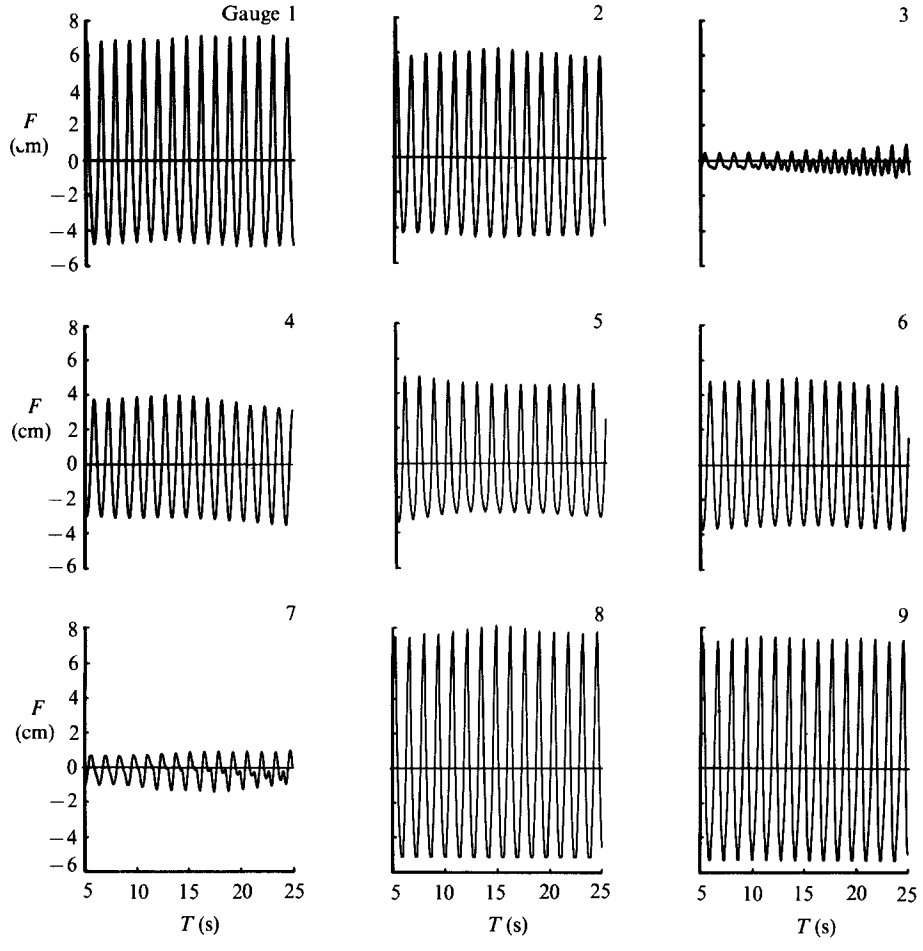

FIGURE 8. Wave profiles for each of the nine gauges in experiment KP3007.

	Theoretical				Measured		
Experiment	$-b$	λ	k	σ	k^2	$(l/k)^2$	$f_{\max}$
KP1007	6.20	0.55	0.900	0.37	0.810	0.022	0.31
KP1507	5.50	0.50	0.867	0.59	0.752	0.045	0.45
KP2007	5.73	0.40	0.843	0.49	0.711	0.076	0.38
KP3007	5.55	0.25	0.800	0.40	0.640	0.213	0.41
KP4007	5.15	0.16	0.720	0.47	0.518	0.488	0.41
KP1011	4.95	0.40	0.585	0.51	0.342	0.050	0.28
KP1511	4.60	0.35	0.565	0.34	0.319	0.085	0.36
KP2011	4.40	0.23	0.540	0.39	0.292	0.200	0.39
KP3011	4.45	0.12	0.500	0.46	0.250	0.395	0.31
KP1015	3.85	0.34	0.420	0.42	0.176	0.071	0.33
KP1515	3.60	0.15	0.390	0.27	0.152	0.252	0.36
KP2015	3.40	0.11	0.367	0.35	0.135	0.401	0.36

TABLE 2. Dynamical parameters for KP solutions of genus 2 in each experiment, normalized r.m.s. error σ between KP solutions and measured waves, and the measured values of the three parameters required to be small for the formal validity of the KP model

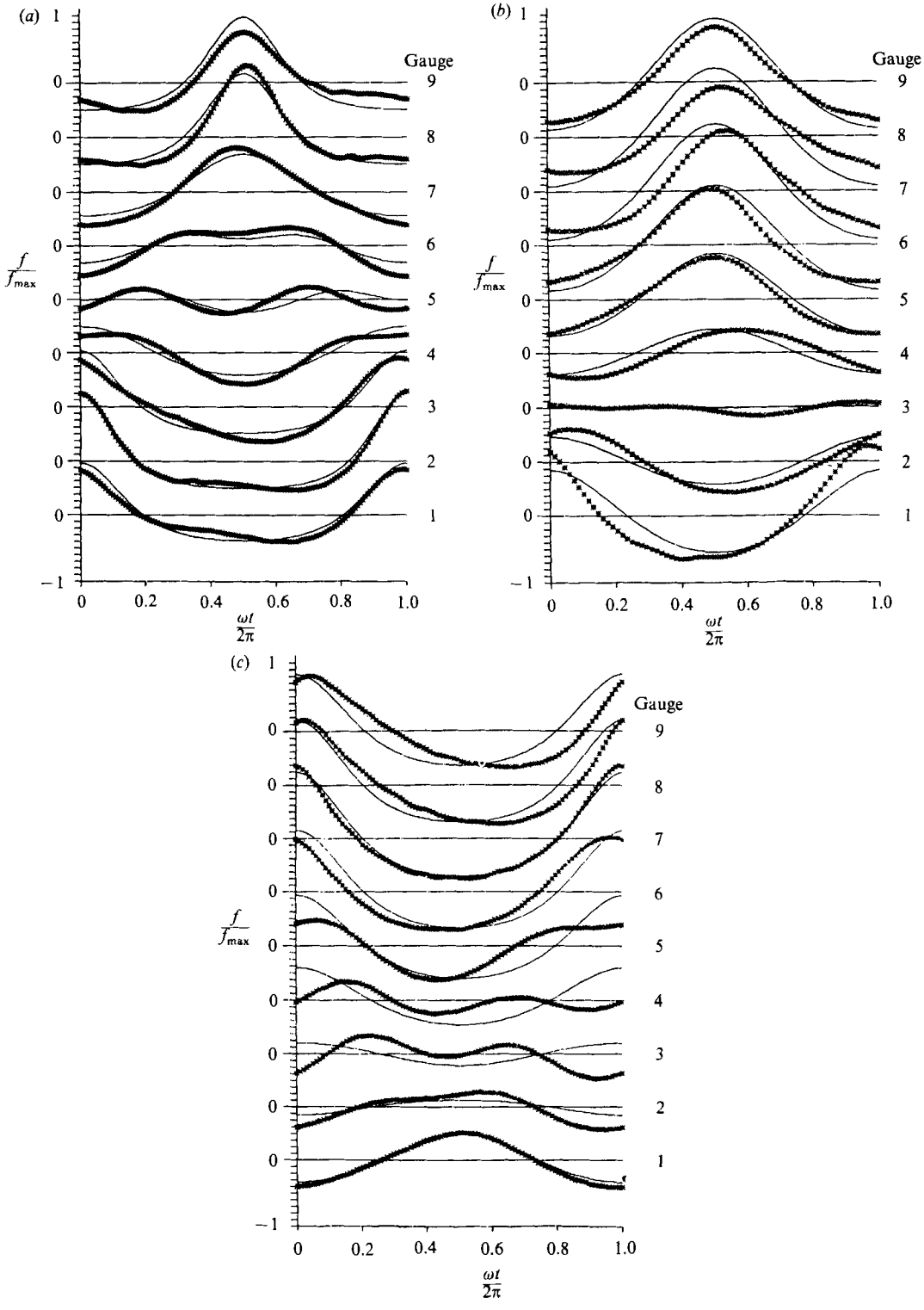

FIGURE 9. One-dimensional slices through the two-dimensional surface patterns showing ——, theoretical and ***, experimental wave profiles at the nine gauges. (*a*) Experiment KP1515; (*b*) experiment KP1007; (*c*) experiment KP1011.

The best agreement between theoretical and measured data occurred in experiment KP1515, which is shown in figure 9(*a*). This excellent agreement resulted in a normalized r.m.s. error $\sigma = 0.27$, which is nearly equivalent to that obtained for genus-1 waves when the basin was calibrated (see §3.2 and figure 6). The fairly large value of σ for the excellent agreement shown in figure 9(*a*) is a consequence of our normalization; recall that this error measure should not be considered in terms of percentage error. The slight discrepancies in wave amplitudes, asymmetries of the measured waves, and nodal arrival times are consistent with those observed for the cnoidal waves in figure 6. Note that adjustment of five parameters in the genus-2 solution of figure 9(*a*) is sufficient to obtain good agreement with the measured waves at all nine gauge sites.

Experiment KP1007 of figure 9(*b*) shows differences in nodal arrival times between the measured and theoretical waves at nearly all gauge sites. There are also significant differences between measured and predicted wave amplitudes, especially in the saddle region. These errors are reflected in the higher r.m.s. error $\sigma = 0.37$; they are typical of experiments in the middle of our measured error range. (A perspective view of the theoretical solution for this experiment is given in figure 2 while an overhead photograph of the experimental waves is presented in figure 7*c*.) Note that gauge 3 is located at a theoretical node of the wavefield which is nearly an experimental node as well.

Experiment KP1011 of figure 9(*c*) is typical of those showing poorest agreement between genus-2 solutions and measured waves. The major contributions to the higher r.m.s. error arise in saddle region where theoretical and experimental waves are almost 180° out of phase and differences between predicted and measured wave amplitudes are significant. Regardless of these discrepancies, the qualitative agreement of KP theory over the full range of data shown in figure 9 is striking.

4.3. *Linear superposition of genus-1 waves*

As already described in §3.2, the experimental waves presented in §4.2 result from the oblique interactions of two genus-1 waves input at the wavemaker. In order to examine the importance of nonlinear interactions in these experiments, another theoretical solution, based on the linear superposition of two cnoidal waves, was compared with the measured waves in the three experiments presented in figure 9. (Recall that these waves essentially span the error range of our twelve experiments.) The cnoidal wavetrains for each experiment were assumed to be directed at angles $\pm\beta$ to the X-axis as listed in table 2, to have a period equal to that of the measured waves, and to have a maximum amplitude of half that of the measured waves. (The last assumption is consistent with forcing the KP solution to agree with the maximum measured amplitude in the surface-fitting algorithm.)

In terms of σ, the KP model always proved better than (or equivalent to) linear superposition of cnoidal waves for each of the experiments. (This was also true for each of the nine wave records within each experiment.) In experiment KP1515, we found $\sigma = 0.44$ using linear superposition compared to $\sigma = 0.26$ for KP theory. In order to illustrate the differences between KP theory and linear superposition, perspective views of both theoretical solutions for the parameters of experiment KP1515 are shown in figure 10; the water surface is pictured for two spatial periods. The dominant feature of both solutions is the large-amplitude crest in the interaction region where the underlying waves overlap spatially. However, the wave crests in the KP solution are longer and more uniform in amplitude than those resulting from linear superposition. More importantly, the longer interaction regions of the KP

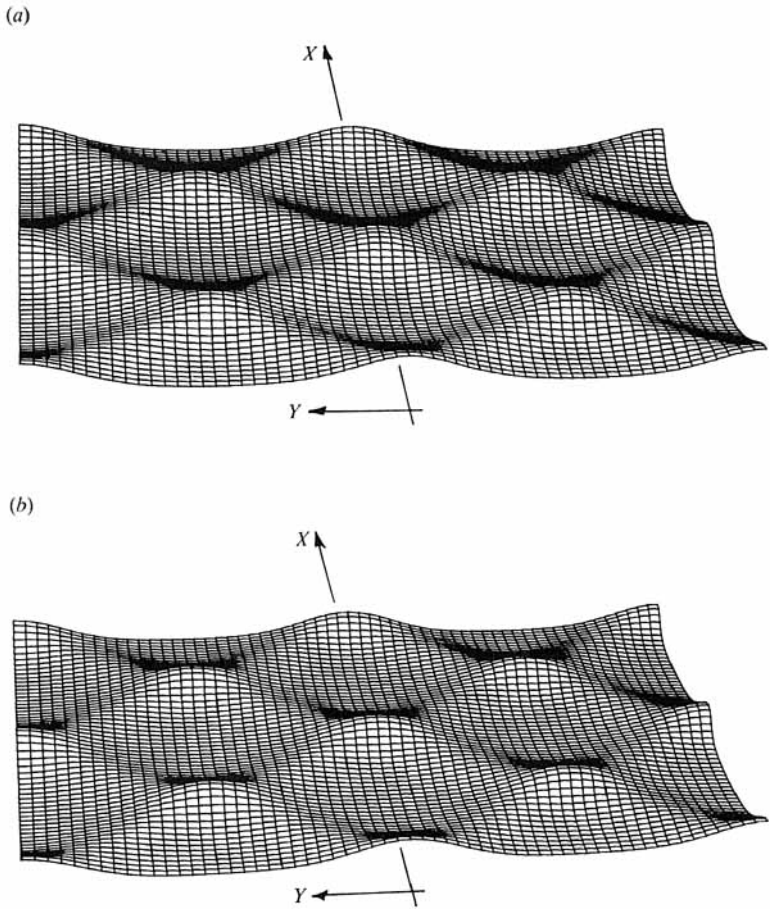

FIGURE 10. Perspective views of computed wavefields for experiment KP1515. (*a*) Linear superposition of underlying cnoidal wavetrains; (*b*) KP solution of genus 2.

solution are accompanied by phase shifts of the underlying (saddle) waves as they enter and exit an interaction region. These phase shifts are described by Segur & Finkel (1985) who showed that they become more pronounced in the soliton limit $b \to 0$, in which an explicit formula relates them to the magnitude of the parameter λ. They are a distinguishing feature of the KP model, with no counterpart in linear superposition. The existence of phase shifts in the measured waves is clear in the overhead photographs of figure 7(*b*, *c*). (Only one saddle region is visible in figure 7(*a*); hence, the phase shifts cannot be detected from this figure; however, they are visible in the video tape of that experiment.)

The results for experiment KP1007 were $\sigma = 0.45$ using linear superposition, compared to $\sigma = 0.37$ using KP theory. The r.m.s. error for experiment KP1011 using linear superposition was $\sigma = 0.54$, which was slightly greater than that ($\sigma = 0.51$) for KP theory. Hence, KP theory consistently predicted the measured waves in these experiments better than a model based on the linear superposition of cnoidal waves. Unfortunately, none of our experiments are near the soliton limit $b \to 0$, in which phase shifts radically alter the KP solutions from those resulting from linear superposition. (Calculations by Segur & Finkel (1985) show that the features of the soliton limit appear for $b \geqslant -1$.) The experiment nearest this limit (KP2015) has

$b = -3.4$, even though the underlying cnoidal waves there have an elliptic modulus $M = 0.97$. We conjecture that KP theory will prove significantly better than linear superposition for modelling water waves nearer the soliton limit.

4.4. *Parameter ranges of KP theory and stability of experimental waves*

As noted in §2, the KP equation becomes asymptotically valid in the limit of $k \to 0$ so that the conditions of (2) are satisfied. (Alternatively, the three parameters of (2) may be replaced by k^2, $(l/k)^2$ and $f_{\max}$.) Actual numerical ranges over which these parameters can be considered small are usually established empirically. In these first experiments with two-dimensional waves, we did not make an extensive effort to determine these parameter ranges; however, acceptable ranges of validity for k^2 and $f_{\max}$ for one-dimensional waves are well estblished in engineering practice (e.g. see Sarpkaya & Isaacson 1981, or the US Army CERC 1984). Weakly nonlinear theories are used up to breaking-wave heights, i.e. $H \approx 0.8D$, while $k^2 < 0.06$ is the accepted range for long-wave dispersion. Neglecting the up/down asymmetry of nonlinear waves in shallow water, the breaking height for one-dimensional long waves corresponds to a breaking amplitude of $f_{\max} \approx 0.6$.

The measured values of the three parameters involved in KP theory for each of our twelve experiments are summarized in table 2. The experimental measures of dispersion are in the range $0.135 \leqslant k^2 \leqslant 0.810$; hence, each experiment involves more dispersion than customarily accepted in engineering practice for the application of long-wave theories. While the good agreement between KP theory and the measured data in KP2015, in which $k^2 = 0.135$, may not seem too surprising, the continued agreement till $k^2 = 0.810$ in experiment KP1007 is noteworthy. The rank ordering of these experiments by r.m.s. error, σ, shows no particular trend in terms of dispersion; in fact, experiment KP1007 is one of the better comparisons.

The maximum amplitudes of the experimental waves were all large, lying in the range $0.28 \leqslant f_{\max} \leqslant 0.45$. Again, there does not appear to be a trend among the experiments between $f_{\max}$ and σ. Indeed, experiment KP1011, which has the smallest amplitude among all the experiments, ranks eleventh among the twelve experiments. This behaviour contrasts markedly with the largest-amplitude experiment (KP1507), which compares worst according to σ. As already noted, there was other experimental evidence that all of the waves in the experiments of series KPxx07 were nearly breaking, even though their relative heights, $0.34 \leqslant H/D \leqslant 0.49$, were substantially below that for breaking one-dimensional waves. Hence, the two-dimensionality of the wave pattern, which is measured by the parameter $(l/k)^2$, may be important in establishing a breaking criterion for these two-dimensional waves, contrary to a prediction by Le Mehaute (1986).

As sought in the original planning of these experiments, the two-dimensionality of the measured waves spans a wide range from $(l/k)^2 = 0.022$ in experiment KP1007 to $(l/k)^2 = 0.488$ in KP4007, in which the crests of the underlying cnoidal waves formed an angle of 54.8°. Even though the restriction of KP theory to weakly two-dimensional waves (i.e. small angles) appears to be violated in many of these experiments, the genus-2 solutions do well. The ranking of experiments by σ shows no particular trend with angles of the underlying waves. Hence, it does not appear that the accuracy of KP theory is particularly sensitive to angles (or two-dimensionality) over the wide range of values in these experiments.

In spite of excessive amounts (from the point of view of KP theory) of dispersion, amplitude, and two-dimensionality in many of these experiments, the waves retained their qualitative structure during propagation over the entire length of the

basin. (This distance corresponded to about 25 wavelengths for the KPxx07 experiments and about 12 wavelengths for the KPxx15 experiments.) All of the waves propagated in a basin where the variations in quiescent water depth were as large as the amplitudes of the generated waves. In other experiments, in which simultaneous breaking of waves occurred in the interaction regions, the waves reformed and continued propagation. This observed behaviour provides qualitative evidence of the stability of these two-dimensional waves. In contrast, Benney & Roskes (1969) showed that one-dimensional (sinusoidal) waves in shallow water were unstable to two-dimensional perturbations, except for a special case of neutral stability at $k = 0.38$. Su *et al.* (1981) provided experimental evidence of shallow-water instabilities for one-dimensional waves. Since genus-2 solutions can contain large regions where the waves are essentially one-dimensional (see figure 2), it is not clear whether the one-dimensional regions will remain stable over long distances of propagation. However, it should be noted that the one-dimensional regions of genus-2 waves approximate cnoidal, rather than sinusoidal, waves; the higher harmonics present in cnoidal waves might provide a stabilizing influence.

5. Summary and conclusions

Twelve experiments were presented in which two oblique cnoidal wavetrains were generated mechanically in a wave basin of (nearly) uniform depth; both wavetrains had the same amplitude and period. These interacting wavetrains produced a wavefield which propagated with practically no change in form; the surface pattern of this wavefield was genuinely two-dimensional and fully periodic, i.e. periodic in two spatial directions and time. The wave patterns were hexagonal in shape, and symmetric about the direction of propagation, which coincided with the bisectrix of the angle formed by the crests of the underlying cnoidal waves input at the wavemaker. These hexagonal wavefields were observed to be stable, retaining their form even up to breaking amplitudes and propagating for distance up to 25 wavelengths in a basin whose depth variations were as large as the wave amplitudes. (These two-dimensional waves were also observed to break at heights substantially smaller than those observed for one-dimensional waves in shallow water.) In most experiments the hexagonal wave patterns were dominated by wave crests normal to the direction of pattern propagation, which we termed interaction regions. These crests were connected by saddle-like waves to complete the hexagonal pattern. Quantitative measurements of the wavefields were obtained from overhead photographs of the surface wave patterns and a linear array of nine wave gauges, aligned perpendicular to the direction of pattern propagation.

The experimental waves were found to be described with reasonable accuracy by a subset of a family of exact solutions of the Kadomtsev–Petviashvili equation known as KP solutions of genus 2. A member of this symmetric subset of genus-2 solutions is completely specified by the choice of five parameters. An algorithm was presented for using the measured data to choose these five parameters in order to obtain a genus-2 solution for each of the twelve experiments. The accuracy of these KP solutions in representing the form of the measured waves was then calculated in terms of a normalized r.m.s. error σ, which was in the range $0.27 \leqslant \sigma \leqslant 0.59$ (perfect agreement between theory and experiments would yield $\sigma = 0$; no theory at all would yield $\sigma = 1$. A calibration of the experimental facility using a single cnoidal wavetrain indicated that a value of $\sigma = 0.24$ was the best that could be expected owing to the depth variations in the wave basin). The accuracy of KP theory

persisted even though many of the experiments were outside the putative range of validity of the KP equation. In particular, both the weakly nonlinear and weakly two-dimensional assumptions underlying the KP equation were violated in some experiments.

The authors gratefully acknowledge the support and cooperation of the Coastal Engineering Research Center, US Army Engineer Waterways Experiment Station in Vicksburg, Mississippi, which made these experiments possible. They also thank Dr A. Finkel for many helpful comments, and the Office, Chief of Engineers, US Army Corps of Engineers for authorizing publication of this research. H.S. acknowledges support from the Army Research Office and the National Science Foundation. J.H. acknowledges support from the Office of Naval Research. We also acknowledge the useful comments of one Journal referee, who remains dissatisfied with our surface-fitting algorithm.

Appendix A. Surface fitting and error measurement

One referee raised serious objections to our algorithm for choosing KP solutions that best-fit experimental data, since it did not incorporate the error measurement σ. It was suggested that we employ a standard regression analysis that would choose the KP solution that minimized σ. Such an analysis would incorporate all of our data, rather than the single datum for the maximum amplitude, and undoubtedly, would lower the values of σ reported in table 2. While regression analysis has obvious merit, we prefer our algorithm for the following two reasons. First, our procedure provides a more severe test of KP theory, since it chooses the KP solution that minimizes one norm of error (the L_∞ norm, which is zero to within the accuracy of our measurements), and then computes error based on a different norm (the L_2 norm, i.e. σ). Second, the L_∞ norm is especially useful in engineering applications where it is often more sensible to choose a design wave whose maximum amplitude agrees with measurements. While regression analysis would minimize σ, the maximum amplitude of the theoretical and measured waves would no longer (necessarily) agree. Regardless of which error measure is minimized, figure 9 shows that KP theory provides a reasonable description of the measured waves.

REFERENCES

Airy, G. B. 1845 Tides and waves. *Encyclopaedia Metropolitana* **5**, 241–396.

Benney, D. J. & Luke, J. C. 1964 On the interactions of permanent waves of finite amplitude. *J. Math. Phys.* **43**, 309–313.

Benney, D. J. & Roskes, G. J. 1969 Wave instabilities. *Stud. Appl. Maths* **48**, 377.

Bridges, T. J. 1987*a* Secondary bifurcation and change of type for three-dimensional standing waves in finite depth. *J. Fluid Mech.* **179**, 137–153.

Bridges, T. J. 1987*b* On the secondary bifurcation of three dimensional standing waves. *SIAM J. Appl. Maths* **47**, 40–59.

Bryant, P. J. 1982 Two-dimensional periodic permanent waves in shallow water. *J. Fluid Mech.* **115**, 525–532.

Bryant, P. J. 1985 Doubly periodic progressive permanent waves in deep water. *J. Fluid Mech.* **161**, 27–42.

Chappelear, J. E. 1959 A class of three-dimensional shallow water waves. *J. Geophys. Res.* **64**, 1883–1890.

Chappelear, J. E. 1961 On the description of short-crested waves. *Beach Erosion Bd. US Army Corps Engrs Tech. Memo.* no. 123, 1–26.

DUBROVIN, B. A. 1981 Theta functions and non-linear equations. *Russ. Math. Surv.* **36**, 11–92.

FUCHS, R. A. 1952 On the theory of short crested oscillatory waves. *Gravity waves. US Natl Bur. Stand. Circ.* no. 521, 187–200.

GORING, D. G. & RAICHLEN, F. 1980 The generation of long waves in the laboratory. *Proc. 17th Intl Conf. Coastal Engrs, Sydney, Australia.*

HSU, J. R. C., SILVESTER, R. & TSUCHIYA, Y. 1980 Boundary-layer velocities and mass transport in short-crested waves. *J. Fluid Mech.* **99**, 321–342.

HSU, J. R. C., TSUCHIYA, Y. & SILVESTER, R. 1979 Third-order approximation to short-crested waves. *J. Fluid Mech.* **90**, 179–196.

KADOMTSEV, B. B. & PETVIASHVILI, V. I. 1970 On the stability of solitary waves in weakly dispersing media. *Sov. Phys. Dokl.* **15**, 539–541.

KORTEWEG, D. J. & VRIES, G. DE 1895 On the change of form of long waves advancing in a rectangular canal, and on a new type of long stationary wave. *Phil. Mag.* **39**, 422–443.

KRICHEVER, I. M. 1977 Methods of algebraic geometry in the theory of non-linear equations. *Russ. Math. Surv.* **32**, 185–313.

LAMB, H. 1932 *Hydrodynamics.* Dover.

LE MEHAUTE, B. 1986 On the highest periodic short-crested wave. *J. Waterway, Port, Coastal, Ocean Engng* **112**, 320–330.

MCLEAN, J. W. 1982*a* Instabilities of finite-amplitude water waves. *J. Fluid Mech.* **114**, 315–330.

MCLEAN, J. W. 1982*b* Instabilities of finite-amplitude gravity waves on water of finite depth. *J. Fluid Mech.* **114**, 331–341.

MEIRON, D. I., SAFFMAN, P. G. & YUEN, H. C. 1982 Calculation of steady three-dimensional deep-water waves. *J. Fluid Mech.* **124**, 109–121.

MELVILLE, W. K. 1980 On the mach reflexion of a solitary wave. *J. Fluid Mech.* **98**, 285–297.

MILES, J. W. 1977*a* Obliquely interacting solitary waves. *J. Fluid Mech.* **79**, 157–170.

MILES, J. W. 1977 *b* Resonantly interacting solitary waves. *J. Fluid Mech.* **79**, 171–179.

ROBERTS, A. J. 1983 Highly nonlinear short-crested water waves. *J. Fluid Mech.* **135**, 301–321.

ROBERTS, A. J. & PEREGRINE, D. H. 1983 Notes on long-crested waves. *J. Fluid Mech.* **135**, 332–335.

ROBERTS, A. J. & SCHWARTZ, L. W. 1983 The calculation of nonlinear short-crested gravity waves. *Phys. Fluids* **26**, 2388–2392.

RUSSELL, J. S. 1844 Report on waves. *Report of 14th Meeting of the British Association for the Advancement of Science*, pp. 311–390. John Murray.

SAFFMAN, P. G. & YUEN, H. C. 1980 A new type of three-dimensional deep-water wave of permanent form. *J. Fluid Mech.* **101**, 797–808.

SARPKAYA, T. & ISAACSON, M. 1981 *Mechanics of Wave Forces on Offshore Structures.* Van Nostrand-Reinhold.

SCHEFFNER, N. 1988 Stable three-dimensional biperiodic waves in shallow water. *Misc. Pap. CERC*-88-4.

SEGUR, H. & FINKEL, A. 1985 An analytical model of periodic waves in shallow water. *Stud. Appl. Maths* **73**, 183–220.

STOKER, J. J. 1957 *Water Waves.* Interscience.

STOKES, G. G. 1847 On the theory of oscillatory waves. *Trans. Camb. Phil. Soc.* **8**, 441–455.

SU, M.-Y. 1982 Three-dimensisonal deep-water waves. Part 1. Experimental measurement of skew and symmetric wave patterns. *J. Fluid Mech.* **124**, 73–108.

SU, M.-Y., BERGIN, M., MARLER, P. & MYRICK, R. 1982 Experiments on nonlinear instabilities and evolution of steep gravity-wave trains. *J. Fluid Mech.* **124**, 45–72.

SU, M.-Y., BERGIN, M., MYRICK, R. & ROBERTS, J. 1981 Experiments on shallow-water wave grouping and breaking. *Proc. First Intl Conf. on Meteorology & Air/Sea Interaction of the Coastal Zone*, pp. 107–112. *The Hague, Netherlands.* Am. Met. Soc.

US ARMY COASTAL ENGINEERING RESEARCH CENTER 1984 *Shore Protection Manual*, vols. 1–3. US Government Printing Office, Washington, DC.